Ionic crystals in a linear Paul trap

M. G. Raizen,* J. M. Gilligan, J. C. Bergquist, W. M. Itano, and D. J. Wineland
Time and Frequency Division, National Institute of Standards and Technology, Boulder, Colorado 80303
(Received 31 October 1991)

We describe a configuration for a linear Paul rf ion trap. This trap can store a long string of ions with a small second-order Doppler shift, comparable to that achieved with a single ion in a quadrupole Paul trap. Crystallized strings of trapped ions, as well as more complicated structures, have been observed in the trap. We report an observation of the 40.5-GHz ground-state hyperfine interval of $^{199}Hg^+$ by microwave-optical double-resonance spectroscopy and discuss prospects for a microwave frequency standard based on a trapped string of ions.

PACS number(s): 32.80.Pj, 32.30.Bv, 95.55.Wk, 36.40.+d

I. INTRODUCTION

Experiments with trapped and laser-cooled ions have been motivated by the possibility for high-accuracy spectroscopy, improved frequency standards, and experiments in fundamental physics. For a large range of spectroscopic experiments, the goal for ion confinement is the Lamb-Dicke regime, in which the extent of the motion of each ion is much less than the wavelength of an atomic transition. For an optical transition this requirement is severe. In a quadrupole rf Paul trap, the total kinetic energy of a single trapped ion can be on the order of the secular kinetic energy, and confinement of a single laser-cooled ion to the Lamb-Dicke regime for an optical transition has been verified spectroscopically in Ba^+ [1,2] and Hg^+ [3]. Laser cooling can significantly reduce the second-order Doppler shift due to the ion motion, which can otherwise limit the accuracy of a spectroscopic measurement. As an example, for a single $^{199}Hg^+$ ion laser-cooled to the Doppler limit [4], the fractional second-order Doppler shift is

$$\langle \Delta\nu/\nu_0 \rangle = -2.3\times10^{-18}$$

(Ref. [5]).

In many experiments it is advantageous or even necessary to work with a larger number of ions. However, in a quadrupole rf Paul trap, two or more ions are pushed by their mutual Coulomb repulsion from the center of the trap to regions where the rf field is stronger. This leads to increased amplitude of the micromotion [6–8], limits the achievable confinement, and may inhibit laser cooling [7,8]. One way to circumvent this problem is to design a trap in which the rf field vanishes along a line instead of at a single point. This goal has led to the development of the linear trap.

The linear-trap design descends from a "racetrack" configuration rf quadrupole trap first used by Drees and Paul for the short-term confinement of an electron-ion plasma [9] and later used by Church to trap atomic ions for longer times [10]. The racetrack trap resembles a quadrupole mass filter bent into a closed path. Charged particles are confined to trajectories along the closed path formed by the electrodes. Dehmelt first suggested using a string of ions in a linear trap to suppress the second-order Doppler shift [11]. In addition to confining the ions radially, it is desirable to fix the axial positions of the ions. In racetrack traps, axial localization can arise from patch effects on the trap electrodes, which pin ions in one region of the trap. Coulomb repulsion among the ions then localizes the remaining ions. The traps described here and in Ref. [12] provide axial confinement with a purposely applied static electric field. This allows the trap to confine the ions more strongly to their axial positions than racetrack traps do and gives more control over the axial positions. The static field weakens the radial confinement, as will be discussed below. Also, racetrack traps can confine both positively and negatively charged particles simultaneously, while traps such as ours, which use static confining potentials, cannot.

Prestage, Dick, and Maleki have trapped a cloud of $^{199}Hg^+$ ions elongated along the axis of a linear trap and have demonstrated a $^{199}Hg^+$ microwave frequency standard with excellent frequency stability [12]. Crystallized strings of laser-cooled $^{24}Mg^+$ ions have been observed in a racetrack-type trap at the Max Planck Institute for Quantum Optics [13]. We have constructed a linear rf trap and observed simple crystallized linear structures of up to 33 $^{199}Hg^+$ ions [14]. By varying the strength of the axial confining potential, we have also observed more complex structures.

In Sec. II we discuss the theory of the linear trap and provide details of our trap. We then present images of trapped crystallized structures of ions and compare these observations with the results of numerical simulations. We next describe an observation of the 40.5-GHz ground-state hyperfine transition using microwave-optical double-resonance spectroscopy with a trapped string of $^{199}Hg^+$ ions and discuss the potential for a microwave frequency standard based on this transition. We conclude with a discussion of future experiments and prospects.

II. THEORY AND DESIGN OF THE LINEAR TRAP

The starting point in the discussion of our linear trap is the quadrupole mass analyzer [15,16]. This device con-

sists of four parallel rods. Typically, each rod has circular cross section in the plane perpendicular to the axis of the trap, as shown in Fig. 1. A time-varying rf potential $V_0\cos\Omega t$ is applied to two opposing rods. The remaining two rods are held at rf ground. The rf electric fields are transverse to the axis of the mass analyzer. The time-varying potential near the axis can be approximated by

$$V=\frac{V_0}{2}\left[1+\frac{x^2-y^2}{R^2}\right]\cos\Omega t\ , \tag{1}$$

where R is the distance from the axis to the surface of the electrodes. For sufficiently high drive frequency Ω, a particle of mass m and charge q moves in an effective pseudopotential

$$\Phi=\frac{qV_0^2}{4m\Omega^2R^4}(x^2+y^2)=\frac{m}{2q}\omega_r^2(x^2+y^2)\ , \tag{2}$$

where

$$\omega_r=qV_0/(\sqrt{2}m\Omega R^2) \tag{3}$$

is the angular frequency of oscillations in the radial direction [12,15,16].

To reduce the anharmonicity of our trap, we chose the rods to have radius $R'=1.03R$. The anharmonicity is minimized with a ratio of 1.146 [17], but is not dramatically worse for our design. A numerical multipole expansion of the field for the geometry of our trap shows that near the axis the harmonic term in the pseudopotential is 1% smaller than that predicted by Eq. (2). The total contribution of anharmonic terms in the pseudopotential, up to order $(r/R)^{10}$, is less than 0.1% of the quadratic term for $(r/R)<0.2$, where r is the distance from the trap axis. While electrodes with hyperbolic cross sections would give a more nearly harmonic pseudopotential, the use of circular rods facilitates construction and is a good compromise since we are primarily interested in confining the ions near the axis. Such a geometry has found wide use as a mass analyzer, but it cannot function as a trap since particles can move freely along the axis.

To confine the ions axially, a static potential can be applied from opposing sides along the axis, creating a region in the center in which particles can be trapped. Figure 2 shows how this is accomplished in our trap. Each of the circular trap rods is divided into two sections of unequal length. The static potential of the longer "central" sections is maintained at ground and a static bias voltage U_0 is applied to the shorter "end" sections. The segmented design divides the trap into three regions along the axis: two end regions where the end segments of two rods overlap the central segments of the other two and a central region where all four central segments overlap. As a function of axial position, the static potential has a minimum in the central region of the trap. The static potential thus provides axial confinement, but is expected to add far greater anharmonicity to the trap potential than does the use of circular rods.

A schematic diagram of the actual trap is shown in Fig. 3. Four circular rods, 12.6 mm long and 1.588 mm in diameter, are aligned with their axes parallel at a radial distance of 1.563 mm from a common axis (the z axis). Each rod is made of two segments of beryllium copper: an end segment 5 mm long and a central segment 7.5 mm long. The central region of the trap, where the four central segments overlap, is 2.5 mm long. The two segments are electrically isolated from each other using spacers of alumina and machinable ceramic, as shown in Fig. 4. This configuration allows independent static potentials to be applied to the segments of the rods. The insulating spacers are hidden from the outside of the rods, as shown in Fig. 4, to avoid perturbations caused by surface charge on the insulators. The ends of the rods are held in two machinable ceramic fixtures (not shown), which are themselves held together by four outer support rods (also not shown). The fixtures were coated with titanium, except where the trap electrodes are held, and grounded in

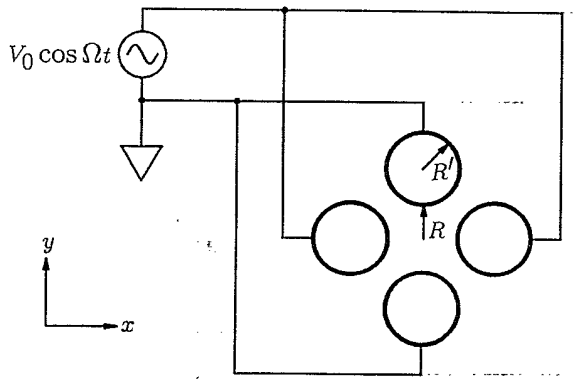

FIG. 1. Cross section of a linear quadrupole trap. An alternating rf voltage $V_0\cos\Omega t$ is applied to a pair of diagonally opposite rods. The other pair of rods is maintained at rf ground. In the actual trap, the radius R' of the rods is 0.794 mm, 1.03 times the distance R (0.769 mm) from the trap axis to the surface of the rods.

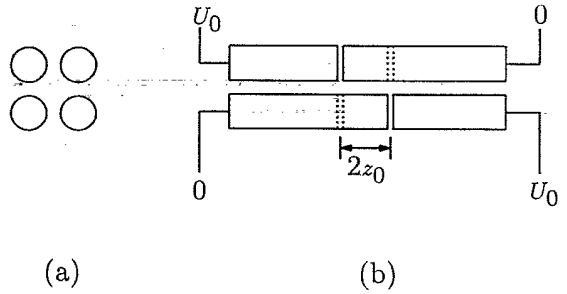

FIG. 2. (a) End view and (b) side view of the linear trap, showing how the axial confining potential is applied. For simplicity, the rf potentials are not indicated on this figure. Each trap rod is divided into two sections that are rf common and held at different static potentials. The dashed lines show the divisions between the sections of the rear rods (which are hidden behind the front ones). The short segments of the rods are held at a positive static potential U_0 and the long segments at static ground, as indicated for the front rods. With this arrangement, we create an axially confining potential for positive ions in the region where the four longer segments overlap. In our trap, this region has length $2z_0=2.5$ mm.

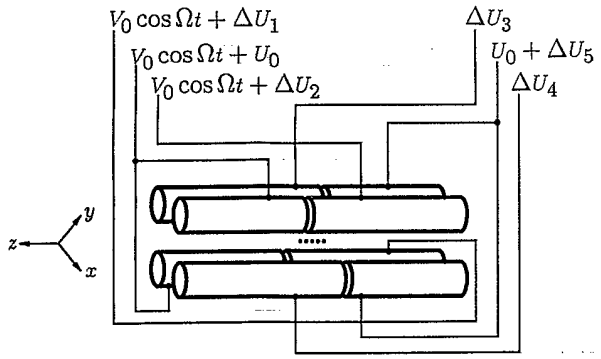

FIG. 3. Linear-trap configuration. An rf voltage $V_0\cos\Omega t$ is applied to diagonally opposite electrodes as shown. The segments of each rod are rf common so that each central segment can be biased at a different static potential ΔU, yet remain at the same rf potential. The end segments of the electrodes are 5 mm long, much longer than the 0.769-mm radial distance from the axis of the trap to surface of the rods, so the rf electric fields in the center section of the trap are nearly parallel to the xy plane. The region in the center of the trap in which the four central segments of the electrodes overlap is 2.5 mm long. To trap positive ions along the z axis, the four central segments are held near static ground potential and a positive static potential U_0 is placed on the end segments. Small potentials $\Delta U_1-\Delta U_4$ can be applied to the central segments to compensate for contact and patch potentials on the electrodes. The axial position of the ions can be varied by applying a bias ΔU_5 to one set of end segments. The ions are detected by an imaging photomultiplier tube that looks along an axis normal to the z axis and 45° to the x and y axes.

order to minimize effects due to charging of exposed insulators.

An rf potential is applied to two opposing rods, while the two other rods are kept at rf ground. The two segments that make up each rod are rf common. The end segment of each rod is biased at a static voltage $U_0>0$, and the central segment is nominally held at zero. This arrangement confines positive ions within the central region of the trap. To compensate for contact and patch potentials on the trap electrodes, there are provisions for applying small static bias potentials ($\Delta U_1-\Delta U_4$ in Fig. 3) to the central segments of the individual rods and to one pair of end segments (ΔU_5).

The rf voltage is supplied by a helical resonator, which acts as a resonant transformer with a 40:1 turns ratio. To allow the different segments of the rods to have different static potentials while remaining at the same rf potential, the secondary winding of the helical resonator is a trifilar coil, whose three filaments supply the voltages $V_0\cos\Omega t+\Delta U_1$, $V_0\cos\Omega t+U_0$, and $V_0\cos\Omega t+\Delta U_2$, as shown in Fig. 3. The rf-grounded rods are capacitively coupled to one another. The resonator produces up to about 700 V amplitude at its 12.7 MHz resonant frequency when driven with about 5W. The high-voltage output is monitored with a capacitive voltage divider, which has been calibrated with 10% accuracy.

Because there is so little symmetry to the trap, describing the static potential in detail would require a full three-dimensional numerical solution. However, the region of interest is near the midpoint of the trap axis, a saddle point of the static potential. In this region the static potential can be approximated by the harmonic potential

$$\phi_s=\frac{\kappa U_0}{z_0^2}[z^2-\tfrac{1}{2}(x^2+y^2)]$$
$$=\frac{m}{2q}\omega_z^2[z^2-\tfrac{1}{2}(x^2+y^2)]\,, \tag{4}$$

where z_0 is half the length of the central region of the trap ($z_0=1.25$ mm for our trap), κ is a geometric factor ($\kappa\approx 0.31$ for our trap; see below), and

$$\omega_z=(2\kappa qU_0/mz_0^2)^{1/2} \tag{5}$$

is the angular frequency of axial oscillations in the trap. The factor κ depends on the geometry of the trap, and hence will vary with z_0, so the secular frequency does not scale simply as $1/z_0$. The pseudopotential well in the radial direction is weakened by the addition of the static potential and is given by

$$\phi_r=\frac{m}{2q}(\omega_r^2-\tfrac{1}{2}\omega_z^2)(x^2+y^2)$$
$$=\frac{m}{2q}(\omega_r')^2(x^2+y^2)\,, \tag{6}$$

where

$$\omega_r'=(\omega_r^2-\tfrac{1}{2}\omega_z^2)^{1/2} \tag{7}$$

is the angular frequency of radial oscillations in the presence of the static potential.

The radial size of the trap was chosen to allow confinement of Hg^+ ions near the Lamb-Dicke regime for a 194-nm optical transition. We define the Lamb-Dicke regime by the criterion that the rms motion of each ion be less than $\lambda/2\pi$, where λ is the wavelength of

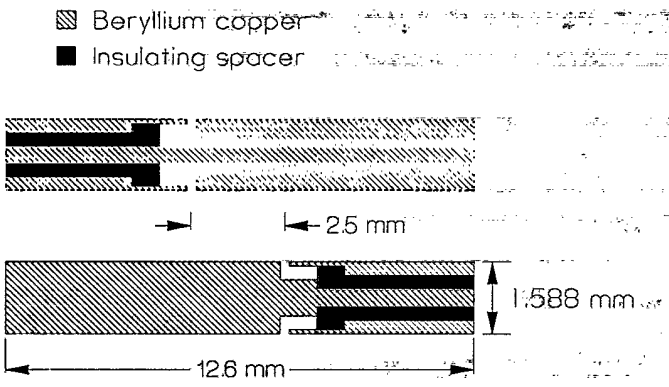

FIG. 4. Section through two trap rods (the front rods in Fig. 2). The end segment of each trap rod is a sleeve that fits over an insulating spacer, which in turn fits over an extension of the central segment. The insulating spacer is completely hidden from the outside of the rod to prevent surface charge on the insulators from perturbing the trap potential.

the transition. Lamb-Dicke confinement in the radial direction is expected for a 12.7-MHz rf drive with an amplitude V_0 of 1.1 kV applied to the trap rods, assuming that the ions have been cooled to the 1.7-mK Doppler limit (this limit applies when motion along each axis is cooled equally [4]). Axial confinement is typically achieved with a static voltage U_0 of 1 V or less. Extrapolating from measured axial secular frequencies, we expect that a static potential of about 400 V would confine the axial motion of a single ion to the Lamb-Dicke regime at the Doppler limit of laser cooling.

III. ION CRYSTALS IN THE LINEAR TRAP

The trap is located in a vacuum chamber maintained at a base pressure of about 10^{-8} Pa (1Pa$\approx$7.5 mTorr) by a sputter ion pump. To load $^{199}Hg^+$ ions into the trap, the pump is turned off and neutral ^{199}Hg vapor (isotopic purity 91%) is bled into the vacuum chamber to give a pressure of approximately 10^{-6} Pa. Neutral atoms in the trap are ionized by electron bombardment from a field emission point. After the trap is loaded, the pump is turned on to return the chamber to near its base pressure. The ions are laser-cooled using the $6s\ ^2S_{1/2}\rightarrow 6p\ ^2P_{1/2}$ transition [3]. A few microwatts of 194-nm laser radiation is sufficient to cool the ions.

Because optical pumping between hyperfine levels of the $^{199}Hg^+$ ion can inhibit laser cooling, two lasers at 194 nm are required. Figure 5 shows the hyperfine levels for the $^2S_{1/2}$ and $^2P_{1/2}$ states of $^{199}Hg^+$ in the absence of a magnetic field. The ions are cooled and detected using a laser (laser 1 in Fig. 5) that is tuned slightly below resonance on the

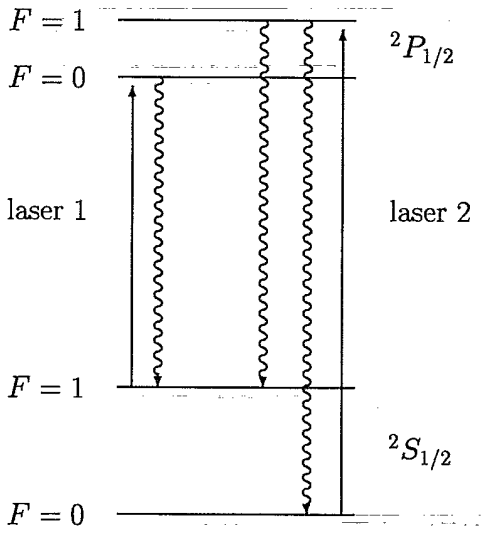

FIG. 5. Energy-level structure for the $6s\ ^2S_{1/2}$ ground state and $6p\ ^2P_{1/2}$ state of $^{199}Hg^+$ near zero magnetic field. The $^2S_{1/2}(F=0)-(F=1)$ hyperfine splitting is 40.5 GHz, and the $^2P_{1/2}(F=0)-(F=1)$ hyperfine splitting is 6.9 GHz. The intervals are not drawn to scale. Lasers 1 and 2 are used for cooling, optical pumping, and detection, as described in the text.

$$^2S_{1/2}(F=1)\rightarrow {}^2P_{1/2}(F=0)$$

transition. This is a "cycling transition," since selection rules require that the ions in the $^2P_{1/2}(F=0)$ level decay only to the $^2S_{1/2}(F=1)$ level. Ions are detected by collecting photons scattered as the ions cycle on this transition. Laser 1 can also weakly excite the

$$^2S_{1/2}(F=1)\rightarrow {}^2P_{1/2}(F=1)$$

transition (the laser frequency is detuned 6.9 GHz from this resonance, whose natural linewidth is $\gamma/2\pi=70$ MHz). From the $^2P_{1/2}(F=1)$ level, the ions can decay to the $^2S_{1/2}(F=0)$ level. This decay path acts to optically pump the ions into the $^2S_{1/2}(F=0)$ level, and ions in this level are not cooled by laser 1. To prevent optical pumping into the $^2S_{1/2}(F=0)$ level, a second laser (laser 2 in Fig. 5) is used to repump ions from the $^2S_{1/2}(F=0)$ level into the $^2S_{1/2}(F=1)$ level via the $^2P_{1/2}(F=1)$ state. Laser 2 is offset about 47.4 GHz to the blue of laser 1, putting its frequency near the

$$^2S_{1/2}(F=0)\rightarrow {}^2P_{1/2}(F=1)$$

resonance. In addition to the above considerations, it is necessary to prevent pumping into the $^2S_{1/2}(F=1,m_F=\pm 1)$ levels. To this end, we apply a magnetic field of approximately 5×10^{-4}T (5G) at about 45° to the electric-field vector of the laser radiation.

The laser is directed through the trap at an angle of approximately 9° from the trap axis in order to cool both radial and axial motion. At this angle, the theoretical Doppler limit of laser cooling is about 1.1 mK for the axial motion and 24 mK for the radial motion [4]. Fluorescence is collected by a fast lens system that produces an image, magnified 22 times, on the front surface of an imaging photomultiplier tube. The spatial resolution of the lens and detector system, defined as the full width at half maximum of the image of a single localized ion, corresponds to 6 μm at the center of the trap. The imaging system looks along an axis normal to the trap axis and at 45° to the x and y axes. At the Doppler limit of laser cooling described above, the rms secular motion along the z axis is calculated to be 1.4 μm for $\omega_z/2\pi=25$ kHz, the smallest secular frequency used in these experiments, so the extent of the secular motion of the ions is less than the spatial resolution of the detector. As the secular frequency is increased, the ions are pushed closer together along the trap axis. For sufficiently high secular frequencies, the ion spacing will decrease below the 6-μm spatial resolution of the imaging system and we will be unable to resolve the individual ions. With two ions in the trap, this should occur at a secular frequency of about $\omega_z/2\pi=400$ kHz.

The temperature of the ions was not measured spectroscopically [3], but we can place an upper bound on the temperature by noting that the images of the ions were about 6 μm full width at half-maximum. We think that this width is due largely to the spatial resolution of the imaging system, but even if the width were entirely due to motion of the ions, we would have $z_{\rm rms}\approx 3\mu m$, from which $T_z\approx 5$ mK for $\omega_z=25$ kHz. If the sizes of the im-

ages of the ions were primarily due to thermal motion, the images would be elliptical, since the secular frequencies in the radial and axial directions are different. The lack of eccentricity in the images supports our supposition that the widths are due to the imaging system and, hence, that the axial temperature is significantly less than 5 mK for $\omega_z = 25$ kHz.

The secular frequencies of the ions are measured by applying a drive to the trap electrodes and observing a drop in the fluorescence as the drive sweeps through resonance [18]. The drop in fluorescence when the amplitude of the secular motion increases is due to the combined effects of the ion's motion taking it out of the laser beam and of Doppler shifts detuning the ion resonance. These measurements permit a quantitative comparison between the observed ion configurations and numerical simulations. The secular frequencies were measured at several different rf and static voltages and showed the expected functional dependence on the voltages. The measured values for the axial secular frequency ω_z were proportional to the square root of the static voltage. The constant κ in Eq. (5) was determined from the measured secular frequencies to be 0.31 with an uncertainty of about 10%. The unperturbed radial secular frequency ω_r was determined from the measured secular frequencies ω_r' and ω_z using Eq. (7). The values for ω_r were proportional to the rf voltage and were consistently 17% ± 10% lower than predicted by Eq. (3), where the uncertainty is dominated by a systematic error in measuring the rf voltage applied to the trap. For very small axial voltages (less than about 100 mV), the effects of local static fields, due to surface charge or patch potentials on the electrodes, make it difficult to characterize the axial potential.

By varying the neutral Hg background pressure and the duration and intensity of the electron bombardment when loading the trap, we can capture different numbers of $^{199}Hg^+$ ions. We have observed single ions and crystalline structures of up to 33 ions, as well as much larger clouds that did not crystallize. The simplest crystalline configuration of ions is a linear string, which is obtained when $\omega_r' \gg \omega_z$. We have observed crystallized linear strings of 2 to 33 ions.

Figure 6 shows images of linear crystals containing 15 and 33 ions. The number of ions we can observe in such crystals is limited by our ability to image the entire string while resolving the individual ions. Large strings, such as the string in Fig. 6(b), are longer than the approximately 200-μm-long region in which the laser intersects the trap axis, and it is not possible to illuminate the whole string at once. To obtain this picture, it was necessary to sweep the position of the laser beam back and forth to illuminate the whole string. A more powerful laser could illuminate a larger area with sufficient intensity to observe the ions easily. Alternatively, more ions could be confined within the illuminated region by increasing ω_z, but the imaging optics cannot resolve ions less than about 6 μm apart, so this approach would require improved imaging optics. We have formed crystallized strings with enough ions that when the spacing between the ions was sufficient for the imaging system to resolve them, the strings were longer than the field of view of the imaging

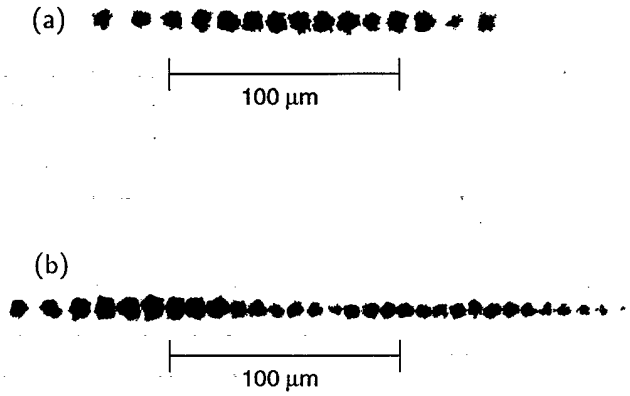

FIG. 6. (a) A picture of a linear crystal of 15 ions. (b) A picture of a linear crystal of 33 ions. This string was longer than the region of the trap axis illuminated by the cooling laser. To obtain an image of the entire string, it was necessary to sweep the laser beam back and forth.

system (about 300μm). The fact that only part of the string was illuminated by the cooling laser did not seem to inhibit cooling and crystallization, although when much larger clouds of ions were trapped, crystallization was not observed. A limitation to forming extremely long strings may be our inability to compensate for the effects of local perturbations to the static potential due to patch fields or surface charge. In the present trap, static potentials can be independently applied to three of the four trapping rods to compensate for such perturbations. This technique works well for short strings, but as the length of the string approaches the radial dimension of the trap (about 750 μm), the patch fields may vary over the length of the string. In this case, we expect the static compensation to be less effective.

Figure 7(a) shows the measured positions of eight ions in a string and the positions calculated by a numerical simulation. The simulation, performed with no adjustable parameters, determines equilibrium positions for the ions by minimizing the potential energy of a given number of particles in harmonic radial and axial wells, with Coulomb repulsion between the particles. The secular frequencies used for the simulation were determined by scaling previously measured secular frequencies by the static and rf voltages applied to the trap. The linear configurations of ions are quite insensitive to the radial secular frequency, because the ions are confined to the axis of the trap.

The ions can be pushed into planar or three-dimensional configurations by increasing ω_z relative to ω_r'. The simplest structure beyond a linear string is a planar zigzag. Figure 8 shows such a structure composed of 11 ions (10 $^{199}Hg^+$ ions and 1 impurity ion, which did not fluoresce). We think that the impurity ion is another isotope of mercury, which would be consistent with the 91% isotopic purity of the mercury vapor used to load the trap. This structure was obtained by lowering the rf voltage on the trap. Figure 7(b) compares the measured positions of the ions to the predictions of a calculation. To obtain agreement between the zigzag configuration

and a numerical simulation with 11 $^{199}Hg^+$ ions, it was necessary to introduce into the calculations an *ad hoc* asymmetry of about 20% between the secular frequencies in the x and y directions. This azimuthal asymmetry forces the ions to lie in a plane; without it, the calculation predicts a quasihelical structure that disagrees significantly with the observed ion positions. The axial secular frequency ω_z and the smaller radial secular frequency ω_y' were determined by scaling previously measured secular frequencies by the voltages present on the trap when this crystal was observed. The larger radial secular frequency ω_x' was set to $1.2\omega_y'$.

The source of the azimuthal asymmetry in the potential well is not known. One possible cause is unequal contact or patch potentials on the trap rods. Another possible cause is the azimuthal asymmetry of the static trapping field. At the geometric center of the trap the static field should be the same in the x and y directions. However, the position of the ions along the axis was not necessarily at the center and varied from load to load. We suspect that this was due to surface charge deposited during loading. When the ions are not at the midpoint of the trap axis, there is a quadrupole component to the radial static field, which breaks the azimuthal symmetry of the

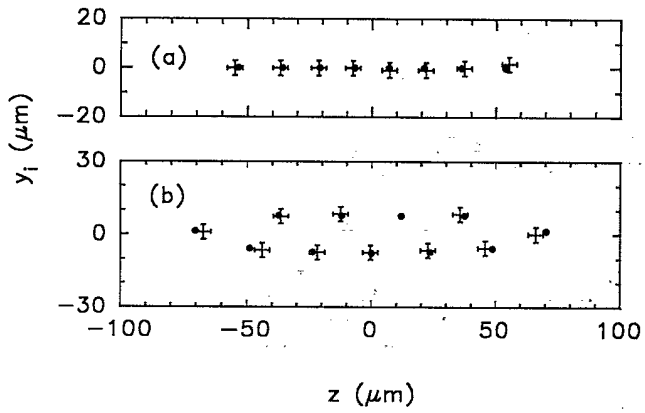

FIG. 7. Observed positions of ions in the trap (crosses) and positions predicted by a numerical simulation (circles). The arms of the crosses extend to the half-maximum intensity points of the images (about 4 μm radius). The coordinates are as in Fig. 3: z represents the displacement along the trap axis and y_i represents the projection of the radial displacement onto the image plane. (a) A linear crystal of 8 ions. The secular frequencies used for the calculation are $\omega_r'/2\pi=435$ kHz and $\omega_z/2\pi=41.7$ kHz. These frequencies were determined by scaling secular frequencies measured under different conditions by the voltages present on the trap when this image was acquired. (b) A nonlinear crystal of 11 ions. One site in the crystal was occupied by an impurity, which did not fluoresce. An asymmetry between the x and y directions was introduced *ad hoc* to make the results of the calculation agree with the data. This asymmetry makes $\omega_x'=1.2\omega_y'$ and confines the structure to the yz plane. The secular frequencies used for the calculation are $\omega_x'/2\pi=92.4$ kHz, $\omega_y'/2\pi=77$ kHz, and $\omega_z/2\pi=31$ kHz. The frequencies ω_y' and ω_z were determined by scaling frequencies measured under different conditions by the voltages present on the trap when this image was acquired.

FIG. 8. A picture of a crystal of 11 ions in a zigzag configuration. The crystal consists of 10 $^{199}Hg^+$ ions and 1 impurity ion, which did not fluoresce. This is the same crystal shown in Fig. 7 (b).

effective radial potential given by Eq. (6). In the case of Fig. 7(b), the axial secular frequency is approximately 40% of the mean radial secular frequency, and it seems plausible that the quadrupole asymmetry could produce the observed planar structure. However, further work is required to characterize the asymmetry more completely.

The observed crystalline structures are closely related to the structures predicted for cold ions in storage rings [19]. With many ions and small ω_r', we have observed complex crystallized structures which appear to be nonplanar and require further study. To conduct a systematic and quantitative study of two- and three-dimensional crystallized structures, we will have to eliminate the azimuthal asymmetry from our trap or characterize it more completely.

IV. MICROWAVE-OPTICAL DOUBLE RESONANCE

A string of cold ions is of great interest for high-resolution spectroscopy and improved frequency standards. With imaging techniques, each ion can be treated as an independent atomic clock. Using Dehmelt's "electron shelving" technique, we should be able to detect the clock transition with 100% efficiency in each ion [1,3,20,21]. This would make the signal nearly immune to fluctuations arising from, for example, fluctuations in the laser intensity.

Consider a clock that uses the Ramsey separated-field method in the time domain to interrogate the clock transition at angular frequency ω_0. The clock transition is excited by two phase-coherent pulses of radiation, each of duration ΔT_R, separated by a time T_R ($\Delta T_R \ll T_R$). By probing the clock transition on each side of the Ramsey peak, we can obtain an error signal to correct the average frequency of an oscillator to match the atomic resonance ω_0 [16,22]. The fractional frequency stability of such a locked oscillator, as characterized by the two-sample Allan variance [23], is

$$\sigma_y(\tau)=(\tau N T_R \omega_0^2)^{-1/2} , \tag{8}$$

where τ is the averaging time ($\tau > T_R$) and N is the number of atoms. Thus, it is advantageous to use large N, ω_0, T_R, and τ. The trap environment can make long interrogation times T_R possible ($T_R=550$ s has been achieved with $^9Be^+$ ions in a Penning trap [22]).

To achieve high accuracy, we must minimize and account for external perturbations due to electric, magnet-

ic, and gravitational fields. These include ion-trap and ion-ion interactions, collisions with neutral background atoms, external magnetic and electric fields, and gravitational red shifts [5,6,11,24,25]. For a microwave transition in a cold string of $^{199}Hg^+$ ions, it should be possible to reduce these effects to the point where the uncertainty in the transition frequency is dominated by the uncertainty in the second-order Doppler shift. When the secular motion is cooled to the Doppler limit, the fractional second-order Doppler shift can be as low as -2×10^{-18} [16]. This limit can be realized if the ions lie exactly along the axis of the trap, where the rf trapping fields approach zero. In this case, the kinetic energy in the rf micromotion is about equal to that in the secular motion, and the two make approximately equal contributions to the second-order Doppler shift. If contact or patch potentials on the trap electrodes push the ions away from the region of minimum rf field, the kinetic energy in the micromotion, and hence the second-order Doppler shift, can be significantly greater. Thus, in a clock based on this trap, it will be necessary to adjust the static shimming potentials $\Delta U_1-\Delta U_4$ on the trap rods to compensate for contact and patch potentials.

This potential for very high accuracy has led us to investigate the possibility of a microwave frequency standard based on the 40.5-GHz ground-state hyperfine splitting of $^{199}Hg^+$ with a trapped and laser-cooled string of ions. This transition is, to first order, independent of magnetic field at zero field. For a Ramsey interrogation time of $T_R=100$ s and $\omega_0/2\pi=40.5$ GHz, the frequency stability of a clock "ensemble" of $N=50$ ions would be

$$\sigma_y(\tau)=5.5\times10^{-14}\tau^{-1/2},$$

where τ is expressed in seconds.

As a first step toward this goal, we have recently observed the 40.5-GHz ground-state hyperfine transition of a string of $^{199}Hg^+$ ions by microwave-optical double resonance. In this preliminary observation the total fluorescence of the entire string of ions was detected. Fluctuations in the fluorescence from the ion cloud due to amplitude and frequency noise in the cooling and detection laser were too large for us to detect transitions with 100% efficiency. To describe the measurement sequence, we rely on the discussion of laser cooling and optical pumping given in Sec. III and on the level diagram shown in Fig. 5. To prevent optical pumping into the $^2S_{1/2}(F=1,m_F=\pm1)$ levels of the ground state, it was necessary to apply a magnetic field while the cooling lasers were on. However, we also wanted to observe the microwave transition in near-zero magnetic field, so we used two sets of Helmholtz coils. One set was used to nearly cancel the ambient magnetic field in the trap. No magnetic shielding was used. The residual field near the trap was measured to be approximately 1.6×10^{-5} T (0.16 G). A second set of coils produced the field used to prevent optical pumping when laser 1 was on. The current in the second set of coils was switched off and on to switch the field between 1.6×10^{-5} T and approximately 5×10^{-4} T, respectively. The sequence of the experiment is the following.

(a) Initially, lasers 1 and 2 and both sets of Helmholtz coils are on. This allows the ions to be laser-cooled.

(b) Laser 2 is turned off and the ions are optically pumped by laser 1 into the $F=0$ ground state.

(c) Both lasers are turned off. The second set of Helmholtz coils is switched off, reducing the magnetic field to approximately 1.6×10^{-5} T. The

$$^2S_{1/2}(F=0)\rightarrow{}^2S_{1/2}(F=1)$$

ground-state hyperfine transition is driven using the Ramsey method with two microwave pulses, each of duration ΔT_R and separated by a time T_R. The pulse duration ΔT_R is adjusted to be close to the value that gives a $\pi/2$ pulse at the resonant frequency. At the microwave intensities used here, this was obtained for $\Delta T_R=0.13$ s.

(d) the second set of Helmholtz coils is switched back on, laser 1 is turned on, and the number of photons counted by the detector during a gate time is recorded. Only those ions that made the microwave transition are in the $(F=1)$ hyperfine level of the ground state, so only those ions fluoresce. With laser 2 off, these ions are eventually optically pumped into the $(F=0)$ level and cease fluorescing. The gate time is chosen to be shorter than the optical pumping time. In these experiments, gate times of 30–40 ms were used (at the laser intensity used here, the time constant for optical pumping was about 50 ms).

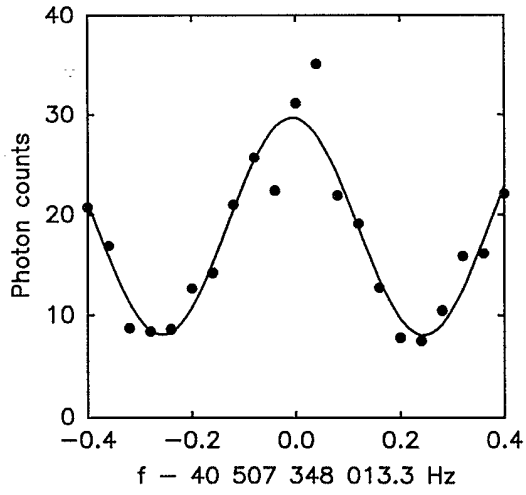

FIG. 9. Microwave-optical double-resonance spectrum of the

$^2S_{1/2}(F=0)\rightarrow{}^2S_{1/2}(F=1)$

ground-state hyperfine transition in $^{199}Hg^+$ at 40.5 GHz. This figure shows the central peak of a Ramsey resonance, obtained using the measurement sequence described in the text, with a linear string of eight ions in the trap. The circles represent the measured fluorescence, and the solid line is a cosine function fit to the data. For this measurement $T_R=1.8$ s, $\Delta T_R=0.130$ s, and each point is the average of 27 measurements. Including time for cooling, pumping, and detection, each measurement cycle takes about 3 s.

At the end of this sequence, the frequency of the microwave source is stepped, and the sequence is repeated. The results of many scans of the microwave frequency are averaged together. Several sets of data were acquired, with T_R ranging from 0.32 to 1.8 s. The result of one observation, using a string of eight ions, is shown in Fig. 9. The linewidth, determined by a least-squares fit of a cosine function to the data, is 251 ± 6 mHz, giving a fractional resolution of 6.2×10^{-12}, and showing good agreement with the 254-mHz theoretical linewidth for the 0.13-s pulse duration and 1.8-s free precession time used in this measurement. Because we did not take advantage of the nearly 100% detection efficiency that would be possible if we counted the fluorescence from each ion individually, the signal-to-noise ratio is limited by fluctuations in the ion fluorescence caused by intensity and frequency noise in laser 1. With this amount of noise, the difference between a pure cosine and the central lobe of a Ramsey profile is insignificant. The amount of technical noise from laser 1 also means that the stability figure given by Eq. (8) is not applicable.

V. FUTURE PROSPECTS

Future experiments will measure the fluorescence from each ion individually. It should be possible to detect the microwave transition with 100% efficiency if the fluorescence detection efficiency is high enough that when laser 1 is turned on, many photons are detected from each ion in the $(F=1)$ level before it is optically pumped into the $(F=0)$ level. If laser 1 is detuned by half a linewidth from the

$$^2S_{1/2}(F=1)\rightarrow{}^2P_{1/2}(F=0)$$

transition, the number of photons scattered by an ion in the $^2S_{1/2}(F=1)$ level before it is pumped into the $(F=0)$ level is approximately the square of the ratio of 6.9 GHz [the detuning of laser 1 from the

$$^2S_{1/2}(F=1)\rightarrow{}^2P_{1/2}(F=1)$$

transition] to 35 MHz (half the radiative linewidth). This gives about 4×10^4 photons. Therefore, the detection efficiency must be significantly greater than the inverse of this number, 2.5×10^{-5}. If this condition is met, it should be possible to detect the microwave transitions with nearly 100% efficiency. By observing the rate of quantum jumps by a single ion in the trap, we determined the rate at which the ion fluoresced [26], and by comparing this rate to the count rate from the detector, we measured the overall detection efficiency of our present apparatus to be about 1×10^{-4}, which is marginally acceptable.

To reach the very high accuracy which should be possible with such a clock, it will be advantageous to use longer interrogation times. To reduce the effects of collisions with neutral background gas atoms and molecules during long interrogation intervals, we plan to use cryogenic pumping. Although in our preliminary measurements the fluorescence was collected from the entire string, it should be possible to treat each ion as an independent clock, since our imaging system resolves the individual ions in the string. Beyond the applications to high-accuracy spectroscopy, the possibility of confining a string of ions so that each is in the Lamb-Dicke regime should permit experiments in fundamental physics, such as studies of interference, cavity QED, and collective behavior.

ACKNOWLEDGMENTS

We thank Sarah Gilbert and Fred Moore for helpful comments on this paper. This work was supported by the U.S. Office of Naval Research and the U.S. Air Force Office of Scientific Research.

*Present address: Department of Physics, University of Texas at Austin, Austin, TX 78712.

[1] G. Janik, W. Nagourney, and H. Dehmelt, J. Opt. Soc. Am. B **2**, 1251 (1985); W. Nagourney, N. Yu, and H. Dehmelt, Opt. Commun. **79**, 176 (1990).

[2] I. Siemers, M. Schubert, R. Blatt, W. Neuhauser, and P. Toschek (unpublished).

[3] J. C. Bergquist, W. M. Itano, and D. J. Wineland, Phys. Rev. A **36**, 428 (1987); F. Diedrich, J. C. Bergquist, W. M. Itano, and D. J. Wineland, Phys. Rev. Lett. **62**, 403 (1989).

[4] See, for example, W. M. Itano and D. J. Wineland, Phys. Rev. A **25**, 35 (1982); D. J. Wineland and W. M. Itano, Phys. Today **40** (6), 34 (1987).

[5] D. J. Wineland, W. M. Itano, J. C. Bergquist, and R. G. Hulet, Phys. Rev. A **36**, 2220 (1987); D. J. Wineland, W. M. Itano, J. C. Bergquist, J. J. Bollinger, F. Diedrich, and S. Gilbert, in *Frequency Standards and Metrology*, Proceedings of the Fourth Symposium, Ancona, Italy, 1988, edited by A. DeMarchi (Springer, Berlin, 1989), pp. 71–77.

[6] D. J. Wineland, in *Precision Measurement and Fundamental Constants II*, edited by B. N. Taylor and W. D. Phillips, Natl. Bur. Stand. (U.S.) Spec. Publ. No. 617 (U.S. GPO, Washington, DC, 1984), p. 83.

[7] R. G. DeVoe, J. Hoffnagle, and R. G. Brewer, Phys. Rev. A **39**, 4362 (1989).

[8] R. Blümel, C. Kappler, W. Quint, and H. Walther, Phys. Rev. A **40**, 808 (1989).

[9] J. Drees and W. Paul, Z. Phys. **180**, 340 (1964).

[10] D. A. Church, J. Appl. Phys. **40**, 3127 (1969).

[11] H. G. Dehmelt, in *Frequency Standards and Metrology* (Ref. [5]), p. 286.

[12] J. D. Prestage, G. J. Dick, and L. Maleki, J. Appl. Phys. **66**, 1013 (1989); IEEE Trans. Instrum. Meas. **40**, 132 (1991).

[13] H. Walther, in *Proceedings of the Workshop on Light Induced Kinetic Effects on Atoms, Ions, and Molecules*, edited by L. Moi *et al.* (ETS Editrice, Pisa, Italy, 1991), p.

261; G. Birkl, S. Kassner, W. Quint, and H. Walther (private communication).

[14] M. G. Raizen, J. C. Bergquist, W. M. Itano, and D. J. Wineland, in *Quantum Electronics Laser Science,* 1991 Technical Digest Series (Optical Society of America, Washington, DC, 1991), Vol. 11, p. 170; M. G. Raizen, J. M. Gilligan, J. C. Bergquist, W. M. Itano, and D. J. Wineland, J. Mod. Opt. (to be published).

[15] W. Paul, H. P. Reinhard, and U. von Zahn, Z. Phys. **152**, 143 (1958).

[16] D. J. Wineland, J. C. Bergquist, J. J. Bollinger, W. M. Itano, D. J. Heinzen, S. L. Gilbert, C. H. Manney, and M. G. Raizen, IEEE Trans. Ultrason. Ferroelectr. Freq. Control **37**, 515 (1990).

[17] D. R. Denison, J. Vac. Sci. Technol. **8**, 266 (1971).

[18] D. J. Wineland, J. J. Bollinger, and W. M. Itano, Phys. Rev. Lett. **50**, 628 (1983).

[19] R. W. Hasse and J. P. Schiffer, Ann. Phys. (N.Y.) **203**, 419 (1990); R. W. Hasse and J. P. Schiffer, in Proceedings of the Workshop on Crystalline Ion Beams, Wertheim, Germany [Gesellschaft für Schwerionenforschung Report No. GSI-89-10, 1989 (unpublished)]; D. Habs, *ibid.*

[20] W. Nagourney, J. Sandberg, and H. Dehmelt, Phys. Rev. Lett. **56**, 2797 (1986).

[21] T. Sauter, W. Neuhauser, R. Blatt, and P. E. Toschek, Phys. Rev. Lett. **57**, 1696 (1986); T. Sauter, R. Blatt, W. Neuhauser, and P. E. Toschek, Opt. Commun. **60**, 287 (1986).

[22] J. J. Bollinger, D. J. Heinzen, W. M. Itano, S. L. Gilbert, and D. J. Wineland, IEEE Trans. Instrum. Meas. **40**, 126 (1991).

[23] J. A. Barnes *et al.*, IEEE Trans. Instrum. Meas. IM-**20**, 105 (1971).

[24] W. M. Itano, L. L. Lewis, and D. J. Wineland, Phys. Rev. A **25**, 1233 (1982).

[25] D. J. Wineland, W. M. Itano, J. C. Bergquist, J. J. Bollinger, and J. D. Prestage, Ann. Phys. (Paris) **10**, 737 (1985).

[26] W. M. Itano, J. C. Bergquist, R. G. Hulet, and D. J. Wineland, Phys. Rev. Lett. **59**, 2732 (1987).